Intermediate state trapping of a voltage sensor

Jérôme J. Lacroix,[1] Stephan A. Pless,[2] Luca Maragliano,[1] Fabiana V. Campos,[1] Jason D. Galpin,[2] Christopher A. Ahern,[2] Benoît Roux,[1] and Francisco Bezanilla[1]

[1]Department of Biochemistry and Molecular Biology, University of Chicago, Chicago, IL 60637
[2]Department of Anaesthesiology, Pharmacology, and Therapeutics, and Department of Cellular and Physiological Sciences, University of British Columbia, Vancouver, BC V6T 1Z3, Canada

Voltage sensor domains (VSDs) regulate ion channels and enzymes by undergoing conformational changes depending on membrane electrical signals. The molecular mechanisms underlying the VSD transitions are not fully understood. Here, we show that some mutations of I241 in the S1 segment of the Shaker Kv channel positively shift the voltage dependence of the VSD movement and alter the functional coupling between VSD and pore domains. Among the I241 mutants, I241W immobilized the VSD movement during activation and deactivation, approximately halfway between the resting and active states, and drastically shifted the voltage activation of the ionic conductance. This phenotype, which is consistent with a stabilization of an intermediate VSD conformation by the I241W mutation, was diminished by the charge-conserving R2K mutation but not by the charge-neutralizing R2Q mutation. Interestingly, most of these effects were reproduced by the F244W mutation located one helical turn above I241. Electrophysiology recordings using nonnatural indole derivatives ruled out the involvement of cation-Π interactions for the effects of the Trp inserted at positions I241 and F244 on the channel's conductance, but showed that the indole nitrogen was important for the I241W phenotype. Insight into the molecular mechanisms responsible for the stabilization of the intermediate state were investigated by creating in silico the mutations I241W, I241W/R2K, and F244W in intermediate conformations obtained from a computational VSD transition pathway determined using the string method. The experimental results and computational analysis suggest that the phenotype of I241W may originate in the formation of a hydrogen bond between the indole nitrogen atom and the backbone carbonyl of R2. This work provides new information on intermediate states in voltage-gated ion channels with an approach that produces minimum chemical perturbation.

INTRODUCTION

Voltage sensor domains (VSDs) are small structural modules formed by four helical segments, S1–S4, which can detect changes in the membrane electric field and respond to them by undergoing specific conformational changes. VSDs have been identified in Na^+, K^+, and Ca^{2+} voltage-dependent channels and in the recently discovered families of phosphoinositides phosphatases (Murata et al., 2005), and voltage-gated proton channels (Ramsey et al., 2006; Sasaki et al., 2006). These proteins carry out fundamental biological functions such as the generation and propagation of action potentials (Hodgkin and Huxley, 1952), the transduction of electrical signals into chemical information (Murata et al., 2005; Ben-Chaim et al., 2006; Jacobson et al., 2010), and the respiratory burst of the innate immune response (Petheo et al., 2010). The voltage sensor operates by moving charged side chains (gating charges) across a focused electric field (Islas and Sigworth, 2001; Asamoah et al., 2003; Starace and Bezanilla, 2004;

Ahern and Horn, 2005), thereby producing transient gating currents (Armstrong and Bezanilla, 1973). In the *Shaker* K^+ channel, a paradigm for voltage-gated K^+ channel studies, the gating charge originates from four conserved positively charged Arg residues in the S4 helix (R1–R4; Aggarwal and MacKinnon, 1996; Seoh et al., 1996) and a conserved negatively charged Glu residue in the intracellular part of the S2 segment (E2; Seoh et al., 1996).

A large amount of experimental data from electrophysiological, biochemical, spectroscopic, and structural techniques shows that voltage-gating encompasses conformational rearrangements of the S4 helix (Posson et al., 2005; Ruta et al., 2005; Posson and Selvin, 2008) between a "down" (resting) and two distinct "up" conformations for the active or relaxed form, respectively (Villalba-Galea et al., 2008). X-ray structures of voltage-gated K^+ and bacterial Na^+ channels revealed the position of the VSD and the gating charges in an up conformation, which corresponds to either the active or the relaxed state (active/relaxed; Long et al., 2007) or

The Rockefeller University Press $30.00
J. Gen. Physiol. Vol. 140 No. 6   635–652
www.jgp.org/cgi/doi/10.1085/jgp.201210827

635

a preactive conformation (Payandeh et al., 2011). On the other hand, atomic proximity between S4 Arg and S1 and S2 have been found in the resting state by cross-linking experiments (Campos et al., 2007; Lin et al., 2010, 2011).

In contrast, little experimental data exists for intermediate positions of the S4 along the conformational transition pathway associated with voltage activation. Obtaining direct structural data about a transition pathway is exceedingly difficult because any intermediate conformation is necessary transient and short-lived compared with the timescale of the whole process. Such transient states cannot be observed experimentally without perturbing the system. In the case of the voltage sensor, information about the transition pathway has been deduced indirectly from cross-linking and mutational studies of various voltage-gated ion channels. Based on cysteine cross-linking experiments in the bacterial voltage-sensitive sodium channel NaChBac, several ion pairs have been suggested to sequentially form between the S4 gating charges and conserved negative counter charges in S2 and S1 (DeCaen et al., 2008, 2009, 2011). However, a recent study concluded that only a single acidic residue of the three most conserved acidic side chains in S2 and S3, E283 (E1) in S2 of *Shaker* K$^+$ channels, contributes to state-dependent ion pair formation, whereas the two others, E293 (E2) and D316 (D3), are unlikely to do so (Pless et al., 2011b). Recently, a highly conserved Phe aromatic residue located in the S2 segment, Phe233, was proposed to catalyze the transfer of R1–R4 (Tao et al., 2010). However, the role of this residue is likely to assist in transferring only a late charge component, presumably carried by R4 (Lacroix and Bezanilla, 2011).

Ultimately, advancing our knowledge of any complex conformational transition, such as the one taking place within the VSD, is likely to require a combination of both experimental data together with careful computational modeling. In the past few years, several molecular dynamics (MD) studies of the VSD have been conducted (Pathak et al., 2007; Khalili-Araghi et al., 2010; Delemotte et al., 2011; Henrion et al., 2012; Jensen et al., 2012). First and foremost, these studies have been aimed at determining the conformation of the resting state of the VSD, which is not known from x-ray crystallography. Despite the wide variations in force fields and simulation methodologies, it appears that the conformation of the resting state is now the object of a broad consensus (see Vargas et al. in this issue). A second goal of the simulations has been to try map out the conformational transition pathway of the gating transition. On this subject, however, the results from MD must be interpreted with caution, as they are unavoidably burdened by approximations. For example, a number of simulations have been performed with either artificial pulling forces or very strong membrane electric fields in order to accelerate the VSD transition and decrease the computational time. As these may lead to nonphysiological transition pathways, it is necessary to examine these results carefully. An alternative method to determine the transition pathway, used in the present study, is the string method (E et al., 2005; Maragliano et al., 2006; Pan et al., 2008).

Here we show that targeted mutations of the residue I241 in the S1 segment of the Shaker channels positively shift the voltage dependence of VSD movement and alter the functional coupling between VSD and pore domains. Interestingly, we found that the I241W mutation stabilized an intermediate state of the VSD and dissociated the gating charge movement into two approximately equal components well separated in the voltage axis. We further investigated the molecular mechanism responsible for this striking phenotype using electrophysiology and the nonsense suppression approach to incorporate nonnatural amino acids. A computational pathway of the VSD transition complemented with additional MD simulations help visualizing the possible interactions stabilizing the intermediate state revealed by the I241W mutation.

MATERIALS AND METHODS

Mutagenesis and expression in *Xenopus* oocytes

All clones in this study are derived from a cDNA encoding the N-inactivation removed Shaker K$^+$ channel Δ4-46 cloned into the pBSTA vector optimized for expression in oocytes (Starace and Bezanilla, 2001) and carrying or not the mutation W434F producing very fast C-type inactivation (Perozo et al., 1993). Single point mutations were incorporated by PCR using mismatch mutagenic primers (QuikChange; Agilent Technologies). All mutants were verified by sequencing the whole cDNA. Mutated cDNAs were linearized with a unique NotI restriction site (enzyme purchased from New England Biolabs, Inc.) and transcribed into cRNAs using a T7 RNA expression kit (Ambion). 30–50 ng of cRNA were injected into *Xenopus* oocytes, usually 24 h after surgical extraction from adult frogs. Injected oocytes were maintained before recordings in a standard oocyte solution containing 100 mM NaCl, 5 mM KCl, 2 mM CaCl$_2$, and 10 mM Hepes, pH 7.5, supplemented with 50 µg/ml gentamycin for 2–6 d at 16.5°C.

Electrophysiology

Electrophysiology experiments were made using the cut-open voltage-clamp method and at room temperature (18°C) unless otherwise stated. The resistance of the intracellular pipette for the virtual ground feedback was 0.5–0.8 MΩ. Data were acquired at a sampling frequency from 30–100 kHz and filtered online at 5–20 kHz using a low pass Bessel filter mounted in the amplifier (Dagan). Capacitive transient currents were subtracted online using the P/4 method when possible. Data were stored and analyzed using in-house software. All gating current recordings were made with the background mutation W434F. The internal gating current recording solution was 115 mM *N*-methyl-ᴅ-glucamine (NMG) methylsulfonate (MES), 2 mM EGTA, and 10 mM Hepes, pH 7.5, and the external solution contained 115 mM NMG-MES, 2 mM Ca-MES, and 10 mM Hepes, pH 7.5. Gating current time constants were determined by fitting the whole decaying part of the current traces with a single or double exponential function. When a double exponential fit was used, a weighted average time constant was calculated. All gating currents analyses are representative of 4–8 independent experiments. To calculate the mid-point $V_{1/2}^{QV}$

values, the Q-V curves were fitted to a single Boltzmann or a sequential two-Boltzmann function as described previously (Lacroix and Bezanilla, 2011). For ionic current recordings, the external solution contained 11.5 mM K-MES, 103.5 mM NMG-MES, 2 mM Ca-MES, and 10 mM Hepes, pH 7.5, and the internal solution contained 115 mM K-MES, 2 mM EGTA, and 10 mM Hepes, pH 7.5. All ionic currents analyses are representative of 3–6 independent experiments. Conductance-voltage (GV) relationships were obtained by plotting the isochronal tail current amplitude as a function of the depolarizing voltage. To calculate the mid-point $V_{1/2}^{G-V}$ values, the G-V curves were fitted to a single Boltzmann function. For experiments using unnatural amino acids, potassium currents were recorded 18–36 h after injection using an OC-725C voltage clamp (Warner Instruments) and recordings were performed at 20–22°C at a holding potential of −80 mV. Standard Ringers solution was used (mM): 116 NaCl, 2 KCl, 1 MgCl$_2$, 0.5 CaCl$_2$, and 5 Hepes, pH 7.4.

Voltage-clamp site-directed fluorimetry

Oocytes expressing the triple mutant I241W/M356C/W434F were incubated in 0.2 mM dithiothreithiol for 30 min and then labeled with 20 µM of tetramethyl-rhodamine-5-maleimide (TMRM; Invitrogen) for 20 min on ice. Labeled cells were individually mounted on an epifluorescence cut-open oocyte setup and illuminated with a tungsten lamp as described previously (Villalba-Galea et al., 2008). TMRM fluorescence was measured using a 535DF35 excitation filter, a 570 dichroic mirror, and a 595AF60 emission filter. The fluorescence data analyses are representative of five independent experiments.

In vivo nonsense suppression for incorporation of nonnatural amino acids

The in vivo nonsense suppression methodology was performed as described previously (Pless et al., 2011a). A TAG stop codon was incorporated at position 241 or 244 of Shaker H4 with deletion of residues 6–46 to remove N-type inactivation (in pBSTA). The fluorinated Trp derivative F$_4$-Trp (4,5,6,7-F$_4$-Trp) was purchased from AsisChem and 2-amino-3-indol-1-yl-propionic acid (Ind) was synthesized as described previously (Belokon et al., 2004). Unnatural amino acids (aa) were protected with nitroveratryloxycarbonyl (NVOC) and subsequently activated as a cyanomethyl ester, which was then coupled to the dinucleotide pdCpA (Thermo Fisher Scientific). The dinucleotide was ligated to a modified tRNA from *Tetrahymena thermophila* and UV irradiation was used to deprotect the aminoacylated tRNA-aa immediately before co-injection with the channel cRNA into *Xenopus* oocytes. Typically, 100 ng of tRNA-aa and 25 ng of channel cRNA were injected in a 50-nl volume. As control experiments, I241TAG or F244TAG cRNA together with tRNA with no appended aa were injected. Even large (+50 mV) depolarizations produced average currents of only 100 nA for I241TAG and 800 nA for I244TAG (n = 4–5 each), ruling out significant read-through incorporation of endogenous amino acids or the recharging of the tRNA with endogenous amino acids.

Building a VSD conformational transition pathway using the string method

A transition pathway for the conformational change between the down and the up state of the Kv1.2 VSD was computed using the string method with swarms-of-trajectories (Pan et al., 2008). Given a set of "collective variables" z, functions of the system's atomic coordinates, the method represents the pathway connecting two metastable end-point conformations as a chain of M states, or "images" z = {z(1), z(2), …, z(M)}, referred to as a "string." The algorithm consists in relaxing the string until convergence by making small adjustments Δz(i) to the values of the collective variables at each image (i.e., i = 1,…,M). Given a set of collective variables z,

the mean displacements Δz(i) are calculated as the average dynamical drift from an ensemble ("swarm") of unbiased short MD trajectories of length τ, initiated from each of the images. During the string relaxation, images are kept at equal distance in the space of collective variables. This operation prevents that all images return to the stable end-point states, and it is referred to as reparametrization. As end-points for the present application of the string method, we used conformations for the up and down state of the Kv1.2 VSD that were previously equilibrated and relaxed using MD simulation with explicit solvent and lipid membrane (Khalili-Araghi et al., 2010). It is important to note that these MD simulations were started from the up and down state atomic models, respectively, that were generated by Pathak et al. (2007) using the Rosetta-Membrane structure prediction program. The atomic structure of the up state corresponds essentially to the x-ray coordinates of the Kv1.2 channel after it has been completed for missing structural information, whereas the atomic structure of the down state is a model constrained by a wide range of experimental data (Vargas et al., 2011). Further support for the general validity of these starting structures can be found in the Discussion. However, the string method is an optimization algorithm that requires an initial approximate pathway. In the present example, this position was generated by slowly transforming the up configuration to the down conformation using targeted MD (TMD) simulation, i.e., by restraining the system to a RMSD that decreases linearly in time from the difference between the end points to zero. The RMSD was defined using the backbone atoms of helices S1 to S4 and the side chain atoms of residues R1 to R4 and the negative counter charges E0 (E247 in Shaker), E1, E2, and D3. The TMD trajectory lasted 10 ns. As collective variables for the string method we used the cartesian coordinates of the S1 to S4 Cα atoms and the last carbon atoms on the side chains involved in salt bridges, for a total of 429 variables. A set of 32 images was extracted from the TMD trajectory and reparametrized. Each stage of the string relaxation is made of two steps: (1) a brief equilibration of the atomic conformations via restrained simulations at the collective variables values defining the images, and (2) launching from each image a swarm of 20, independent, 5-ps-long, unbiased trajectories. In the present calculation the string reached convergence in ∼70 iterations, after which the path was further refined for 10 iterations using swarms of 50 trajectories each lasting 10 ps. To monitor convergence we calculate, at each iteration, the path-RMSD with respect to the initial path, i.e., the average of the RMSD of each image with respect to the same image in the initial path (see Fig. S2, A and B). A plateau of this quantity means that the path is not changing anymore after updates, apart from small fluctuation due to noise in the calculated quantities. The same atoms used for collective variables definition are used for the path-RMSD calculation.

In silico mutations

Initial conformations for the mutants simulations were generated by scanning the optimized path for the image showing the minimal Cβ-Cζ distance between I177 (I241 in Shaker) or F180 (F244 in Shaker) and the S4 Arg R1–R4. Mutant side chain atom coordinates and structure files were generated using the psfgen plugin in Visual Molecular Dynamics (VMD). Restrained simulations were then performed at the collective variables values that define the selected images. Trajectories lasted 33 ns for I177W (I241W) and I177W/R2K (I241W/R2K), and 20.6 ns for F180W (F244W). Along these trajectories, van der Waals and electrostatic interaction energies were computed between atoms of residues pairs I177/R2 (I241/R2), I177W/R2K (I241W/R2K), and F180W/R2 (F244W/R2).

MD simulation methodology

All MD simulations for the string method as well as for the in silico mutations were performed using the program NAMD

(Phillips et al., 2005) and the CHARMM27 (Mackerell et al., 2004) force field. The system comprises an isolated VSD immersed in an explicit DPPC membrane (Feller, 2000), TIP3P model water (Jorgensen et al., 1983), and counterions for a total of ~94,000 atoms. Periodic boundary conditions, constant temperature, and constant pressure with a fixed cross-sectional area were used. Electrostatic interactions were computed with the particle-mesh Ewald method (Darden et al., 1993). Temperature and pressure were kept at 318 K and 1 atm, respectively, using Langevin dynamics and the Langevin Nosé-Hoover method (Martyna et al., 1994). All simulations were performed at zero applied voltage because the minimal energy path calculated using the string method depends only on the known end conformations (active/relaxed and resting), the membrane voltage having only an impact on the distribution between the two end conformations.

Online supplemental material

Fig. S1 depicts gating current traces and Q-V curve for the mutant I241W/R2Q. Fig. S2 displays the progression of the RMSD with respect to the initial path during the string method MD simulation. We have also made available the pdb trajectory file. Online supplemental material is available at http://www.jgp.org/cgi/content/full/jgp.201210827/DC1.

RESULTS

The I241 mutations impair channel activation

The residue I241 located in the S1 segment of *Shaker* K$^+$ channels (Fig. 1 A) was shown to lie at the membrane–solution interface of the VSD and to reside within atomic proximity of the S4 backbone at the level of R1 in the resting state (Campos et al., 2007). We thus reasoned

that this residue may play a functional role in K$^+$ channel gating. To further investigate the contribution of this residue, we substituted I241 by 13 different residues (T, V, M, L, N, Q, C, G, S, A, F, Y, and W) and measured the voltage dependence of K$^+$ currents of mutant channels. Fig. 1 B shows current traces for the wild-type (WT) and the I241Y channels. This mutant shows a change in its ability to respond to voltage as K$^+$ conductance is seen only at voltages above 0 mV compared with −30 mV for WT. The mid-points ($V_{1/2}$) of the conductance (G) vs. voltage (V) (G-V) curves for all tested I241 mutants spread over a wide range of voltages separated by more than 60 mV (Fig. 1 C). Only three mutant residues show normal G-V curves with $V_{1/2}^{G-V}$ between −20 and −30 mV (I241T, I241V, and I241L). Interestingly, these residues are commonly found with Ile at the position homologous to I241 in other VSDs (Fig. 1 D).

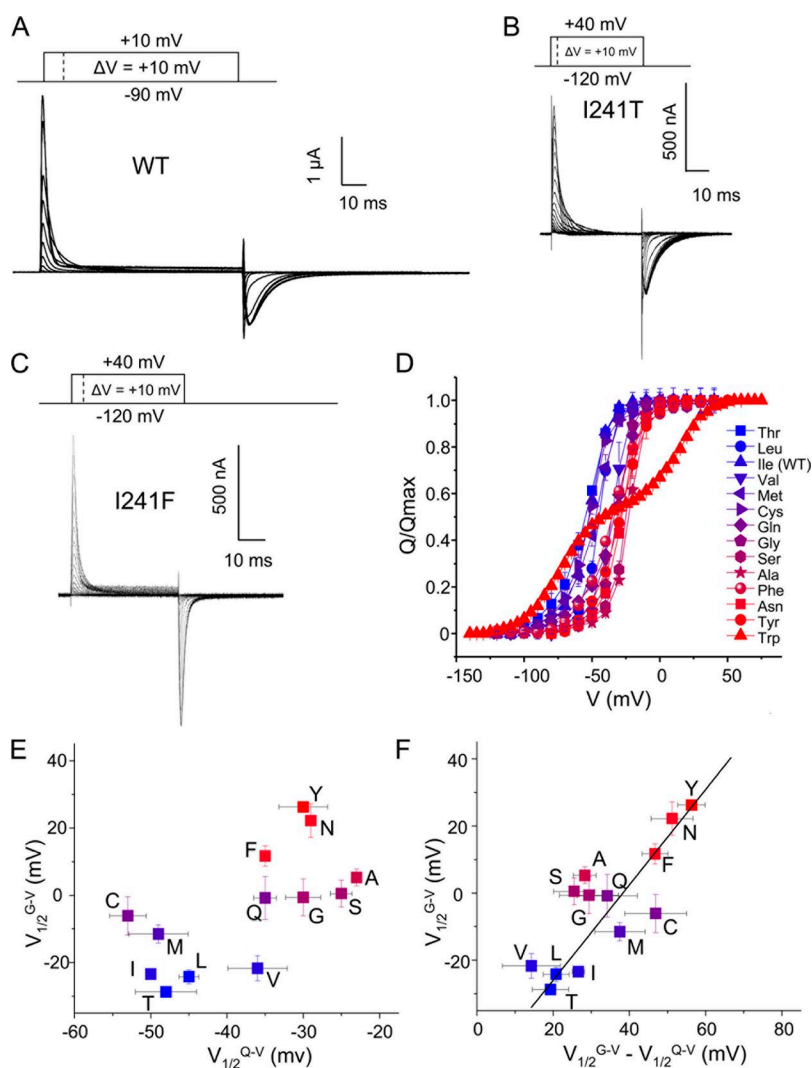### I241 mutations alter VSD movement

To further investigate the molecular origin of the mutant phenotypes, we measured the gating currents of I241 mutants. The gating currents are transient capacitive currents produced by the movement of the gating charges of the VSD within the membrane electric field and are very small compared with the currents resulting from the K$^+$ ions flowing through the pore. To measure gating currents of mutant channels we incorporated the additional mutation W434F, which abolishes K$^+$ conduction
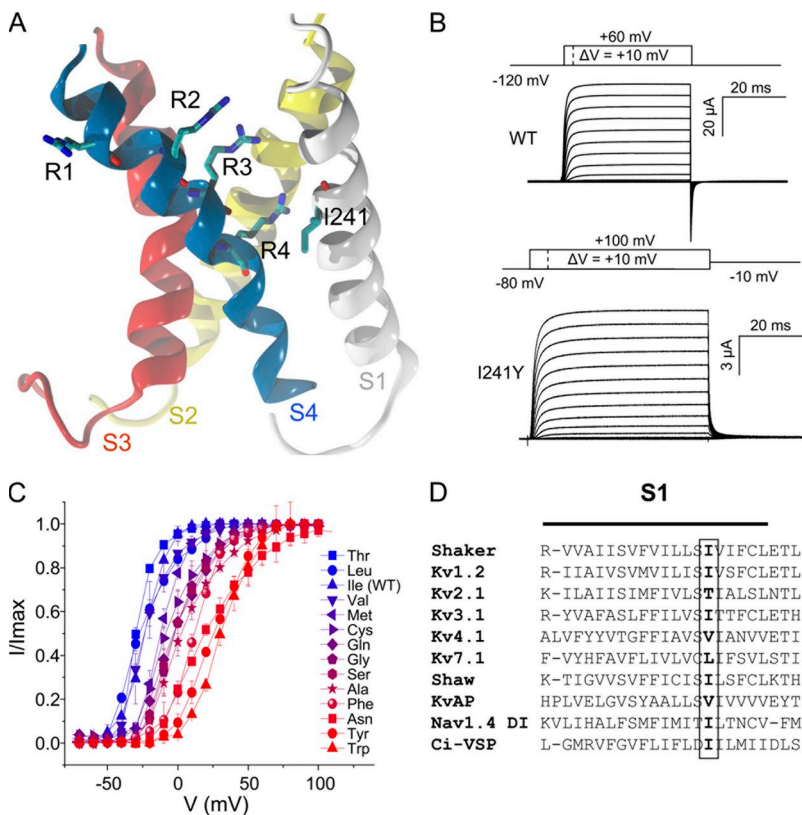
Figure 1. Effect of I241 mutations on Shaker channel gating. (A) Zoomed view of the refined structure of the Kv1.2 voltage sensor (PDB 3LUT; Chen et al., 2010) showing the S1 (white), S2 (yellow), S3 (red), and S4 (blue) helices, the four S4 Arg R1–R4 and the residues I241. (B) Ionic current traces for WT Shaker (top) and I241Y mutant (bottom) recorded using the indicated protocol. (C) G-V curves of Shaker channels as a function of the residue present at position 241. The curves are colored gradually from blue to red relative to their position on the voltage axis from negative to positive potentials. (D) Sequence alignments of the S1 segment (T-Coffee) showing the amino acid at the position homologue to I241 (boxed) in various voltage sensors containing proteins (Shaker, GI: 13432103; K$_v$1.2, GI: 4826782; K$_v$2.1, GI: 4826784; K$_v$3.1, GI: 76825377; K$_v$4.1, GI: 27436981; K$_v$7.1, GI: 32479527; Shaw, GI: 220901931; K$_v$AP, GI: 38605092; Na$_v$1.4 domain I, GI: 292495096 and Ci-VSP, GI: 76253898).

but does not alter voltage sensor movement (Perozo et al., 1993). Fig. 2 (A–C) shows gating current traces for WT and two representative mutants, I241T and I241F, recorded using a classical activation protocol. We calculated the amount of charge displaced (Q) as a function of the pulse voltage (V) by integrating the gating currents produced during activation over time and then plotted the corresponding Q-V curves (Fig. 2 D) using the same coloring scheme as in Fig. 1 C. We could fit the Q-V curve of all mutants with a single Boltzmann equation except for the I241W mutant, which displays a bi-sigmoid Q-V curve (Fig. 2 D). We plotted the $V_{1/2}^{Q\text{-}V}$ values (mid-points of the Q-V) against the corresponding $V_{1/2}^{G\text{-}V}$ values (mid-points of the G-V) for each mutant (Fig. 2 E). The results show that the mutations producing more positive G-V shifts also tend to produce more positive Q-V shifts. However the shifts in the Q-V and G-V curves were not linearly correlated (Fig. 2 E), suggesting that the Q-V shift is not the only mechanism responsible for the G-V shift.

Previous studies have shown that certain mutations in the VSD of ion channels produce dramatic voltage shifts of the ionic conductance with little effect on the bulk of the VSD movement, thus resulting in larger separation of the Q-V and G-V curves in the voltage axis. Some of these mutations have been found to isolate a late gating charge transition near the open state (Smith-Maxwell et al., 1998; Lacroix and Bezanilla, 2011), whereas other mutations did not isolate a detectable charge component (Muroi et al., 2010; Haddad and Blunck, 2011). It is thus possible that the I241 mutations similarly alter a small late gating charge component that is difficult to detect from the gating currents recordings. When the $V_{1/2}^{G\text{-}V}$ values are plotted against the voltage separation between the Q-V and G-V curves ($V_{1/2}^{G\text{-}V} - V_{1/2}^{Q\text{-}V}$), a clear linear correlation is observed (Fig. 2 F; $r^2 > 0.97$). This shows that the voltage dependence of the ionic conductance is quantitatively correlated with the separation between the Q-V and G-V curves in the voltage axis. Such correlation was not observed between $V_{1/2}^{Q\text{-}V}$ and the difference

Figure 2. The I241 mutations alter VSD movement. The figure shows the gating currents traces for WT Shaker (A), the I241T (B), and I241F (C) mutants recorded using the indicated protocols. (D) Q-V curves for the WT and I241 mutants. (E and F) Correlation plots between the midpoints of the G-V ($V_{1/2}^{G\text{-}V}$) and Q-V ($V_{1/2}^{Q\text{-}V}$) (E) and between $V_{1/2}^{G\text{-}V}$ and the difference $V_{1/2}^{G\text{-}V} - V_{1/2}^{Q\text{-}V}$ (F). The line represents a linear fit to the data ($R^2 = 0.97$). The coloring method in D–F is identical to Fig. 1 C.

$V_{1/2}^{G-V} - V_{1/2}^{Q-V}$ (unpublished data). Taken together, these results show that the effects of the I241 mutations is (1) the alteration of the bulk of the VSD movement (Q-V curves) and (2) the alteration of a late VSD transition near the open state, which is responsible for the mechanical coupling between VSD and pore domains.

The I241W mutation immobilizes the S4 movement

The most dramatic effect on channel conductance is produced by the I241W mutation (Fig. 1 C). The gating currents traces measured in the I241W channels during activation show an interruption in the sigmoidal progression of the gating currents not seen in other tested I241 mutants: for the intermediate test-pulse voltages ranging between −50 mV and 0 mV, the OFF gating currents (measured at the same repolarizing voltage) practically overlap (Fig. 3 A). The Q-V curve determined from integrating the ON or the OFF gating currents produced during the activation protocol of Fig. 3 A displays a bi-sigmoidal shape, demonstrating that I241W interrupts the gating charge movement between −50 and 0 mV, isolating two approximately equal charge components (Figs. 2 D and 3 B). By interrupting the gating charge movement, the I241W mutation uses a unique mechanism among the I241 mutations to displace the voltage dependence of the conductance toward more positive voltages.

To investigate whether the I241W mutation alters the physical motion of the S4 helix, we assessed S4 movement in I241W channels by monitoring the quenching of a fluorophore covalently attached to a cysteine inserted at the position of M356C at the top of S4 (Mannuzzu et al., 1996; Cha and Bezanilla, 1997). Fig. 3 C shows the

obtained fluorescence traces which display an interruption in their progression in the same voltage range to where the gating currents are interrupted. Similarly, the fluorescence ($\Delta F/F$) vs. voltage (F-V) curve resembles the Q-V curve of the I241W mutant (Fig. 3 D), confirming that the I241W mutation transiently immobilizes the movement of the S4 helix.

The I241W mutation stabilizes an intermediate state of the VSD

Several mechanisms can be envisaged to explain how the I241W mutation produces a split Q-V curve. Assuming a simplistic 3-state energy diagram for the VSD transition (Fig. 4 A), the I241W mutation could destabilize the active state, thus forcing the VSD to stall into an intermediate state (hypothesis 1, left). This destabilization could be caused by the disruption of residue–residue interactions that normally stabilize the active conformation. The large indole side chain could also produce steric hindrances in the gating charge pathway and produce a large increase of the energy barrier near the active state. This could cause extremely slow gating currents that would be difficult to detect and thus produce an apparent interruption of the charge movement (hypothesis 2, middle). Finally, I241W could interact with neighboring residues in an intermediate conformation, thus stabilizing an intermediate state during the VSD transition (hypothesis 3, right).

As each of these hypotheses lead to experimental predictions, it is possible to determine which one is more likely to explain the behavior of the I241W mutation. Hypothesis 1 predicts that the kinetics of the ionic currents would be normal (with respect to WT) during
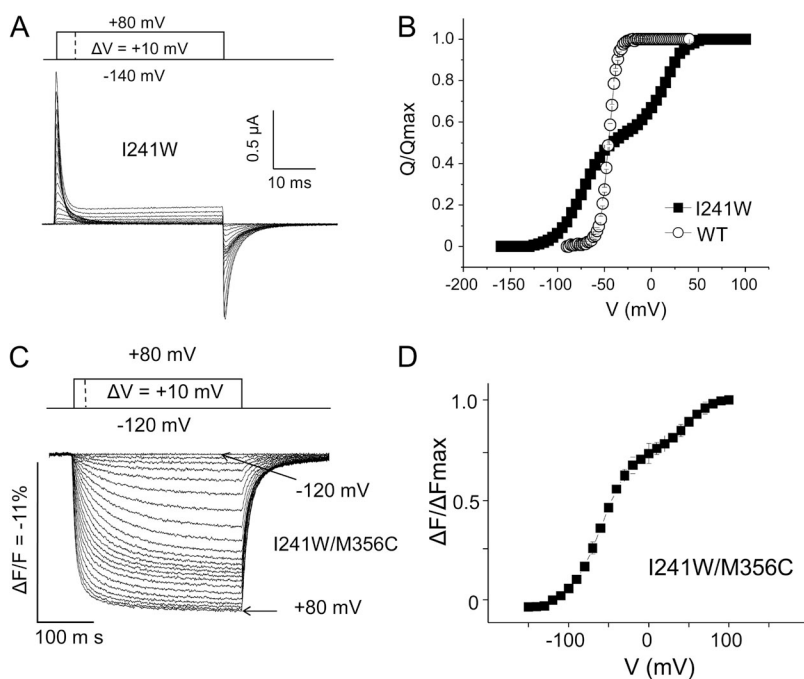
Figure 3. I241W transiently immobilizes S4. (A) Family of gating currents recording for the I241W mutant. (B) Q-V plots for the WT and I241W channels. (C) Family of fluorescence recordings of a tetramethylrhodamine-maleimide fluorophore attached to M356C in the I241W mutant. (D) F-V curve of the labeled I241W/M356C mutant obtained from an isochronal plot of the fluorescence intensities at the end of 300-ms test pulses.

	z_1	z_2	V_1 (mV)	V_2 (mV)	r^2
WT	2.37	4.19	−49.6	−33.9	n.d.
R4K	2.03 ± 0.11	0.93 ± 0.06	−60.7 ± 0.9	46.4 ± 3.2	0.9973
I241W	2.07 ± 0.04	1.91 ± 0.04	−74.4 ± 0.4	9.8 ± 0.4	0.9995
I241W/R1K	1.53 ± 0.04	2.01 ± 0.05	−68.0 ± 0.7	49.6 ± 0.5	0.9995
I241W/R2K	1.62 ± 0.02	1.48 ± 0.02	−59.2 ± 0.3	4.4 ± 0.3	0.9999
I241W/R2Q	1.23 ± 0.07	2.11 ± 0.11	−89.9 ± 2.2	18.8 ± 0.9	0.9974
I241W/R3K	1.84 ± 0.04	2.12 ± 0.04	−93.0 ± 0.5	57.7 ± 0.4	0.9997
I241W/R4K	1.91 ± 0.08	1.75 ± 0.07	−79.1 ± 0.8	88.9 ± 0.1	0.9978
F244W	2.65 ± 0.10	2.29 ± 0.09	−63.4 ± 0.5	−2.3 ± 0.7	0.9993
F244W/R2K	2.61 ± 0.04	2.17 ± 0.03	−53.7 ± 0.2	−12.7 ± 0.2	0.9999
F244W/R3K	2.01 ± 0.09	2.39 ± 0.11	−87.6 ± 1.1	8.6 ± 0.8	0.9978
Deac I241W	2.62 ± 0.19	1.89 ± 0.15	−71.7 ± 0.1	−9.9 ± 1.7	0.9976
Deac F244W	3.56 ± 0.15	2.99 ± 0.15	−64.5 ± 0.4	−15.0 ± 0.6	0.9986
Deac I241W/R2K	2.52 ± 0.12	2.31 ± 0.11	−37.7 ± 0.7	6.2 ± 0.7	0.9994
Deac I241W/R3K	2.25 ± 0.15	2.02 ± 0.14	−91.5 ± 1.2	−20.7 ± 1.4	0.9972

The Q-V curves of the single or double mutants were fitted using a 3-state model equation (see Appendix). The parameters for WT were from a previous work (Bezanilla and Stefani, 1996). The fitted parameters for deactivation (Deac) were obtained from experiments done at 28°C.

activation but much faster during deactivation. In addition, because the thermodynamic equilibrium of the VSD conformations would destabilize the active state, a positive shift of the voltage dependence of the conductance would be observed. Hypothesis 2 predicts that the kinetics would be much slower for both activation and deactivation without modification of the voltage dependence of the conductance. Hypothesis 3 predicts that the kinetics would be slower for activation, unchanged for deactivation and that the voltage dependence of the conductance would be positively shifted. We measured the activation and deactivation ionic currents for the I241W mutant (Fig. 4, B–E) and the kinetic analysis reveals that for activation and deactivation, the time constants (τ) versus V (τ-V) curves of the mutant are positively shifted with respect to WT. In addition, the deactivation
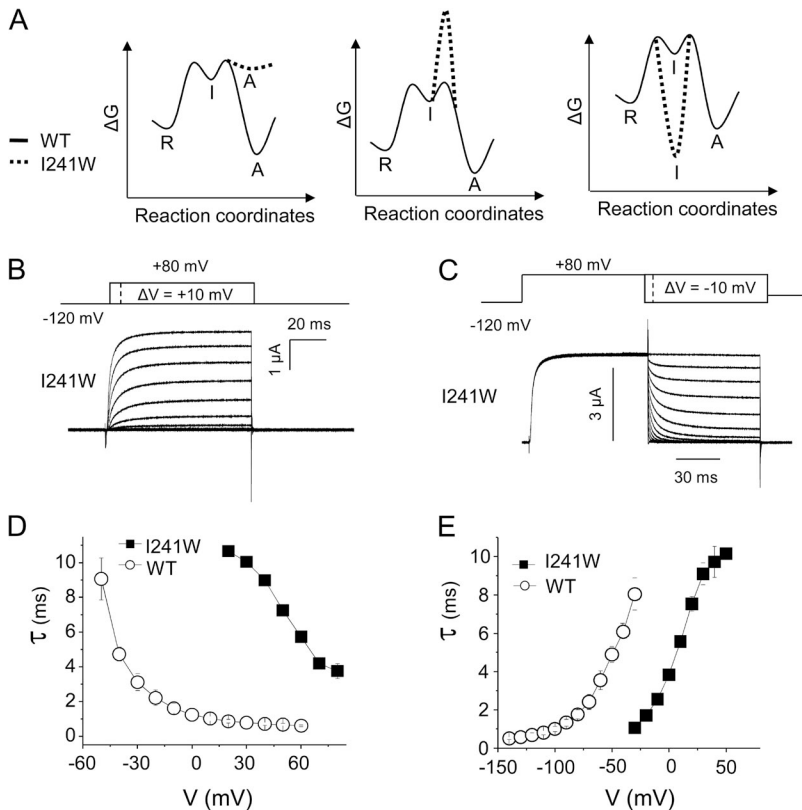
Figure 4. Hypothetical mechanisms for the I241W phenotype. (A) Hypothetical energy diagram of the VSD transitions showing the resting (R), intermediate (I), and active (A) states at a voltage of 0 mV. The dotted lines indicate possible effects of the I241W mutation: destabilization of the active state (left), increase of the energy barrier between the intermediate and active states (middle), and stabilization of the intermediate state (right). (B) Activation ionic currents recordings for I241W channels. (C) Deactivation ionic currents recordings for I241W channels. (D) τ–V plots for WT and I241W channels during activation. (E) τ–V plots for WT and I241W channels during activation.

kinetics of I241W channels approach a value of 0.5–1 ms as the repolarizing potential becomes more negative, which is similar to WT channels whose kinetics approach 0.5 ms at negative potentials. In contrast, for activation, the kinetics of the mutant approach a value of 4 ms at positive potentials, whereas the kinetics for the WT are significantly faster (1 ms). These observations rule out hypotheses 1 and 2 but are in very good agreement with hypothesis 3.
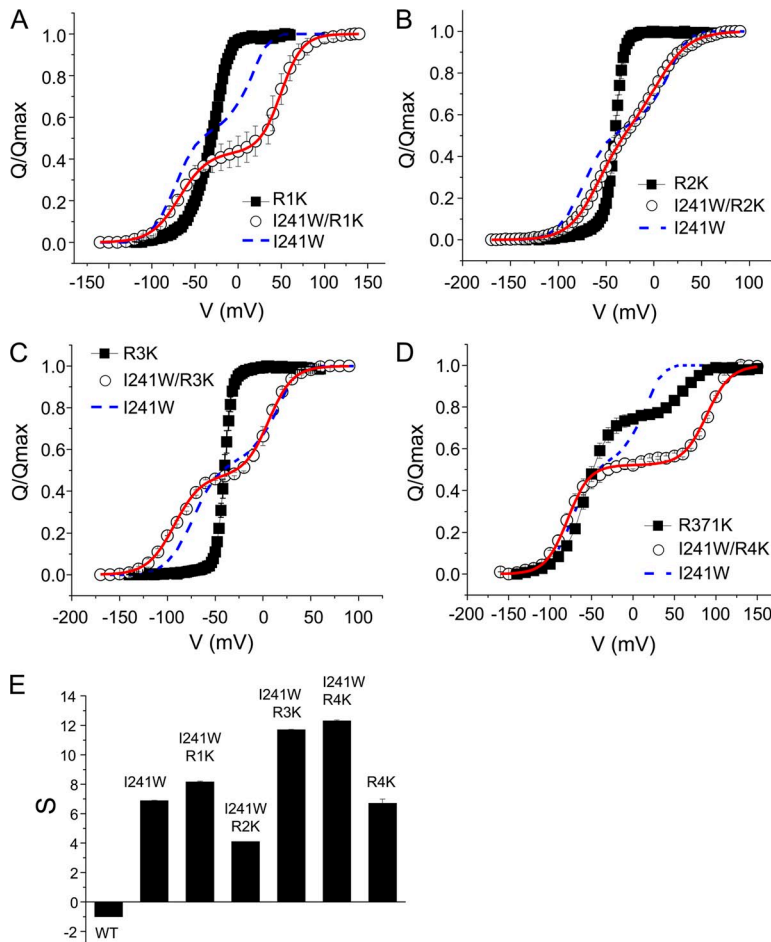
The I241W phenotype depends on the S4 Arg

If a Trp inserted at position I241 stabilizes at intermediate state of the VSD transition, then a possible molecular mechanism could be a transient interaction between I241W and a surrounding residue of the VSD. Because I241 was previously found in atomic proximity to R1 in the resting state (Campos et al., 2007), the S4 Args are good candidates to establish such interactions. To test this hypothesis, we individually mutated each of the four gating charges to Lys in the I241W background and determined the Q-V curves of the corresponding mutants using classical activation pulse protocols. For R1–R3, charge-conserving Arg-to-Lys substitutions produce WT-like gating charge movement (Fig. 5, A–C, squares; Aggarwal and MacKinnon, 1996). However,

the R4K mutation isolates the last 20–25% of the gating charge (Fig. 5 D, squares) as previously reported (Lacroix and Bezanilla, 2011). The results of the double mutants show that I241W/R1K and I241W/R3K exhibit strong Q-V splits similar to that of the I241W mutant but absent in the R1K and R3K mutants (Fig. 5, A and C, circles). The mutant I241W/R4K also displays a Q-V split which approximately corresponds to the addition of the Q-V split seen in the two individual mutations (Fig. 5 D, circles). However, the Q-V split appears diminished in the mutant I241W/R2K (Fig. 5 B, circles). We fitted the Q-V curves of the mutant and WT channels with a sequential 3-state model (Fig. 5, A–D, red traces; see Appendix and the fitted parameters in Table 1).

Assuming a simple 3-state model as shown in Fig. 4 A, the presence of a stabilized intermediate state can be quantitatively determined by calculating the quantity s (see Appendix): $s = e_0 (V_2 z_2 - V_1 z_1)/(kT)$.

A stabilized intermediate state exists if $s \geq 0$. We calculated the value s for each mutant to assess the presence of a stabilized intermediate state in channels bearing the R-to-K substitutions (Fig. 5 E). The data indicate that only the R2K mutation significantly decreases the stabilization of the intermediate state by the I241W mutation (smaller s value).

Figure 5. The I241W phenotype depends on the S4 Arg. The figure shows the Q-V curves measured during an activation pulse protocol for the mutants R1K (A, black squares), R2K (B, black squares), R3K (C, black squares), R4K (D, black squares), and the double mutants I241W/R1K (A, open circles), I241W/R2K (B, open circles), I241W/R3K (C, open circles), and I241W/R4K (D, open circles). In each graph, the dotted blue line represents the Q-V curve for the I241W mutant and the red line represents the fit to a sequential double-Boltzmann equation. (E) Histogram showing the s values ($s = e_0(V_2 z_2 - V_1 z_1)/kT$) (see Table 1). A positive value indicates the presence of a stabilized intermediate state.

Because the neutralizing R2Q mutation produces a bi-sigmoid Q-V curve (Seoh et al., 1996), we wondered how the double mutation I241W/R2Q will affect the gating charge movement. Fig. S1 shows that the Q-V curve for this double mutant displays a very shallow component in the negative voltages that is also seen for the R2Q mutant. However, although the Q-V curve of R2Q channels saturates below 0 mV, the Q-V curve of the double mutant saturates near +50 mV, as for I241W channels. Thus, the Q-V curve of the double mutant I241W/R2Q reproduces the characteristics of the individual mutations, indicating that the two phenotypes appear essentially additive.

The I241W phenotype is maintained during deactivation

We next asked whether the stabilization of the intermediate state by I241W also occurs during deactivation gating. When the deactivation gating currents were measured at a room temperature of 18°C, the gating charge did not appear to be immobilized (Fig. 6 A). However, when the experiment was conducted at 28°C, there was a clear interruption in the progression of the current amplitude as function of the repolarizing voltage (Fig. 6 B). Fig. 6 C shows that the increase of temperature from 18 to 28°C accelerates both activation and deactivation gating currents approximately two- to threefold. Thus, by accelerating the gating currents, the increase in temperature may facilitate the detection of small and/or slow gating charge components which have been previously observed in Shaker deactivation gating (Lacroix et al., 2011). Interestingly, the deactivation τ-V curve measured at 28°C displays a double bell-shaped curve as also seen for the activation τ-V curves (Fig. 6 C). These double bell-shaped curves indicate the presence of two gating charge components well separated along the voltage axis and confirm the stabilization of the intermediate state during deactivation (see Appendix).

The Q-V curve determined by integrating deactivation gating currents at 28°C displays a split separating two unequal charge components of ∼30% and 70%, in contrast to the separation observed during activation (Fig. 6 D). This could indicate that the relative contribution of the gating charge residues to the total charge
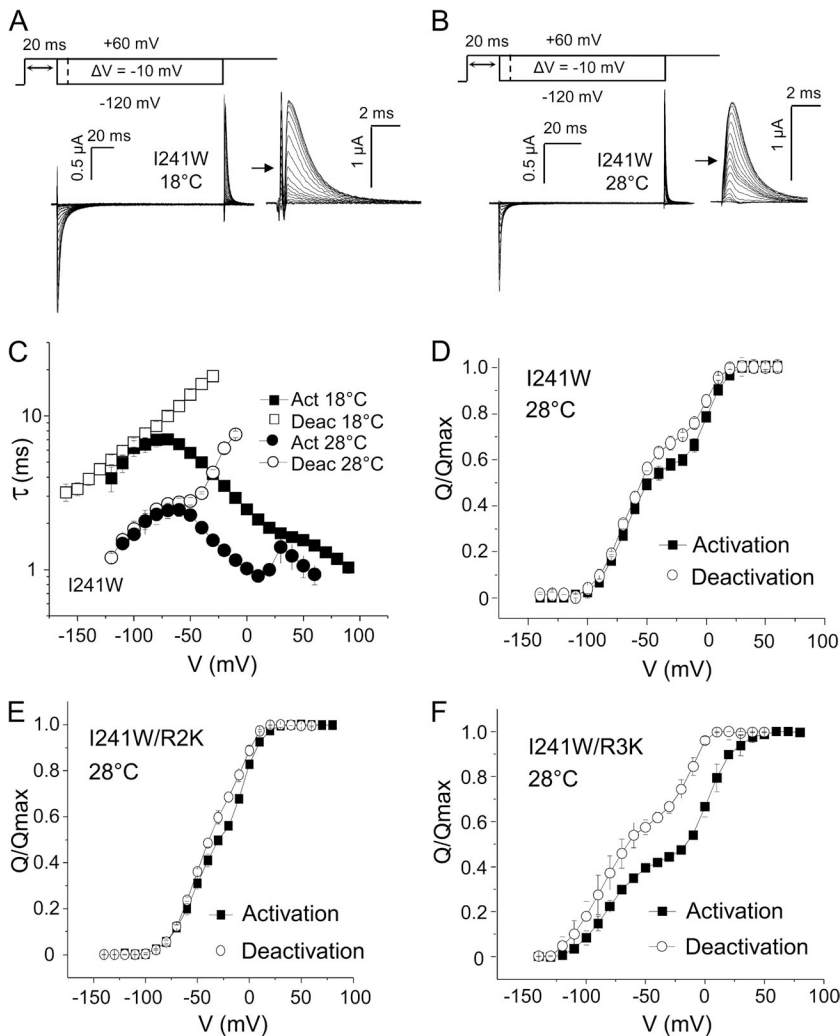
Figure 6. Conservation of the I241W phenotype during deactivation. (A) Deactivation gating current traces recorded in an oocyte expressing I241W channels with the indicated protocol at 18°C. (B) Deactivation gating currents traces recorded in the same cell at 28°C. Traces at the post-pulses in A and B are shown expanded for clarity. (C) τ-V curves of gating currents for the I241W mutant recorded at 18°C (black symbols) or 28°C (open symbols) during activation (circles) or deactivation (squares). (D) Q-V curves for the I241W mutant determined at 28°C during activation (black squares) or deactivation (open circles). (E) Q-V curves for the I241W/R2K mutant determined at 28°C during activation (black squares) or deactivation (open circles). (F) Q-V curves for the I241W/R3K mutant determined at 28°C during activation (black squares) or deactivation (open circles).

varies between activation and deactivation or it could indicate that I241W interacts with R3 during deactivation, isolating a smaller gating component in the positive range compared with during activation. To test this latter hypothesis we compared the activation and deactivation Q-V curves at 28°C for the double mutants I241W/R2K and I241W/R3K (Fig. 6, E and F). The results show that, as during activation, the Q-V split is diminished by the R2K mutation but not by the R3K mutation, indicating that R2 is also involved in the stabilization of the intermediate state during deactivation.

F244W reproduces the phenotype of the I241W mutation

The intermediate state with I241W raises the question whether the insertion of a Trp at nearby positions of I241 could reproduce the characteristics of the I241W mutation. We inserted Trp at the position of I237, one α-helical turn below I241 in S1, and at the position of F244, one α-helical turn above I241. Although we could not measure any detectable gating currents in the I237W mutant, the F244W mutant reproduced most of the I241W phenotype. This mutation produced a split

Q-V curve isolating two nearly identical charge components and dramatically shifted the G-V curve toward positive potentials (Fig. 7, A–C). Also, as in I241W channels, the activation τ-V curve exhibits a double-bell shape, indicative of the separation of two gating charge components (Fig. 7 C). The kinetics of activation and deactivation of the ionic conductance were also similar in amplitude to WT channels albeit shifted positively in the voltage axis (unpublished data). Similarly to the I241W mutant, the insertion of the R2K, but not the R3K, mutation reduced the separation of the gating charge components by the F244W mutation (Fig. 7 D). Finally, the Q-V split produced by the mutation F244W is observed during both activation and deactivation gating (Fig. 7, E and F).

Investigations of the I241W and F244W phenotypes using nonnatural amino acids

As the presence of R2 is required to produce the stabilization by the I241W or F244W mutation, it is possible that the Π electrons of the aromatic Trp are engaged in a cation-Π interaction with the positively charged
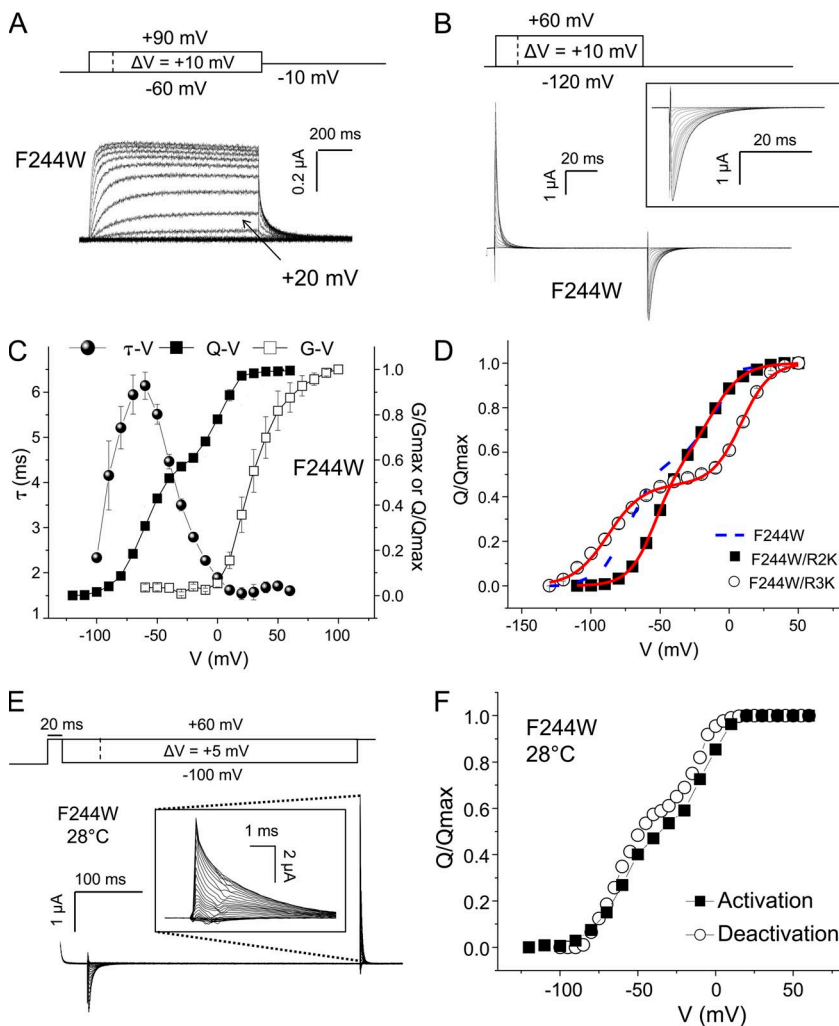
Figure 7. The F244W mutation mimics the I241W mutation. (A) Ionic current traces recorded from the F244W mutant using the indicated activation protocol. (B) Gating current traces recorded from the F244W mutant using the indicated activation protocol. (C) Q-V (black squares), G-V (open squares), and τ-V of gating current (black spheres) plots for the F244W mutant determined from activation protocols. (D) Q-V curves for the double mutants F244W/R2K (black squares) and F244W/R3K (open circles) determined from activation protocols. The dotted blue line represents the Q-V curve of the F244W mutant depicted in C. The red lines represent the fit to a sequential double-Boltzmann equation. (E) Deactivation gating currents measured for the F244W mutant at 28°C. (F) Q-V curves determined at 28°C during activation (black squares) and deactivation (open circles) for the F244W mutant.

guanidinium moiety of Arg (Dougherty, 1996). Such a cation-Π interaction has recently been observed between an S4 charge, likely K374 (K5), and F290W in S2 (Pless et al., 2011b). Previous studies have shown that fluorination of aromatic side chains is a useful tool for testing cation-Π interactions, as each added fluorine should give rise to a step-wise reduction of the cation-Π binding strength (Zhong et al., 1998; Ahern et al., 2006, 2008; Pless et al., 2011b,c). Using the nonsense suppression method, we thus incorporated at position 241 a fluorinated Trp derivative with virtually no cation-Π binding ability, F_4-Trp, or a natural Trp as a control. Because of the relatively low efficiency of the amino acid incorporation using the nonsense suppression technique, the expression level of the modified channels was not high enough to measure gating currents, nevertheless, robust ionic currents could be recorded (Fig. 8 A, left). Our results show that the G-V curve is practically identical whether natural Trp or F4-Trp is present at position I241, thus ruling out the involvement of a cation-Π interaction (Fig. 8 A, right). This result is also in agreement with the observation that the I241W phenotype does not appear to be abolished by the charge-neutralization R2Q mutation.

We next tested the novel side-chain 2-amino-3-indol-1-yl-propionic acid (Ind). This nonnatural amino acid side chain is isosteric to Trp, but the indole nitrogen is directly linked to the α-carbon, such that it can no longer function as a hydrogen bond donor (Fig. 8 B). We found that introduction of Ind at position 241 produces only a moderate +20 mV right shift of the G-V curve

compared with WT instead of the larger +60 mV shift for Trp (Fig. 8 A), suggesting that the large G-V shift caused by the I241W mutation is due, in part, to the presence and location of the indole nitrogen.

We also introduced the nonnaturals F4-Trp and Ind indole derivatives at the positions of F244 and the results indicate that the large G-V shift produced by the F244W mutation unlikely originates from either cation-Π interactions or from the presence of the indole nitrogen (Fig. 8 C).

DISCUSSION

Our study reveals the importance of the residue Ile241 for both the VSD movement and the coupling between VSD and pore domains. Interestingly, the mutations producing the strongest Q-V shifts also produced the weakest mechanical coupling between VSD and pore domains (separation of the Q-V and G-V curves in the voltage axis). We could not find a significant linear correlation between the hydrophobicity, surface or volume of the substituted side chains and the values of the midpoint voltages of the Q-V or G-V curve (unpublished data). Thus the molecular bases underlying most I241 mutant phenotypes—except for I241W—remain unclear.

By systematically screening I241 mutations, we found that the I241W substitution stabilizes an intermediate state of the VSD transition at a point where approximately half of the gating charge has been transferred as assessed by pulsing from negative to positive voltages. The I241W phenotype occurs during activation and
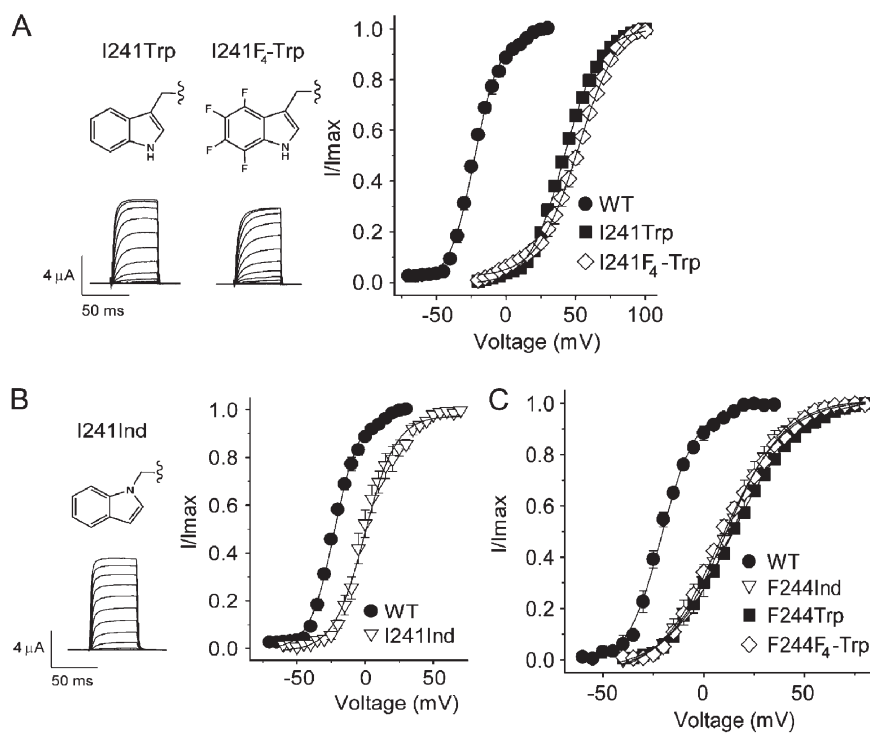
Figure 8. Investigations of the I241W and F244W mutants with nonnatural amino acids. (A, left) Representative current recordings of Shaker channel bearing the natural Trp or the unnatural F_4-Trp side chain at position 241. 50-ms depolarizing pulses were used in 5-mV increments from −20 mV to +100 mV with a holding potential of −80 mV. (Right) G-V curves for WT I241 (black circles, $V_{1/2} = -22.3 \pm 0.6$ mV; $Z = 2.9 \pm 0.3$, $n = 5$), I241Trp (black squares, $V_{1/2} = 41.9 \pm 0.5$ mV; $Z = 1.9 \pm 0.1$; $n = 5$) and I241F_4-Trp (open diamonds, $V_{1/2} = 51.9 \pm 1.3$ mV; $Z = 1.8 \pm 0.2$; $n = 5$). (B, left) Representative current recordings of Shaker channel bearing the Ind side chains at position 241. 50-ms depolarizing pulses were used in 5-mV increments from −60 mV to +60 mV with a holding potential of −80 mV. (Right) G-V curves for WT I241 (black circles, $V_{1/2} = -22.3 \pm 0.6$ mV; $Z = 2.9 \pm 0.3$; $n = 5$) and the I241-Ind mutant (open triangles, $V_{1/2} = 0.6 \pm 2.9$ mV; $Z = 2.5 \pm 0.3$; $n = 6$). (C) G-V curves of WT Shaker (black circles), the F244Trp mutant (black squares), the F244F4-Trp mutant (open diamonds), and the F244-Ind mutant (open triangles).

deactivation gating and in both cases seems to depend on the presence of R2. Interestingly, the insertion of a Trp one helical turn above (position F244) reproduces the phenotypes observed in I241W channels. These observations show that the isolated intermediate state may be physiologically populated by the VSD during activation and deactivation gating and thus suggest the existence of a unique (conserved) structural transition pathway underlying both VSD transitions. In addition, the relative proportions of the gating charge components being separated seems to change depending on whether the charge is transferred during activation or deactivation gating (Fig. 6, D and F; Fig. 7 F). This result suggests that the individual contribution of R1–R4 to the total charge may slightly differ between activation and deactivation and it does not conflict with the conservation of the total charge, which is the sum of the individual charge times the fraction of the field determined between the two end-states of the conformational transition. This observation is also consistent with the prevailing notion that the electrical field is focused across a narrow region inside the VSD. Hence, small differences in the relative contribution of R1–R4 to the gating charge could be produced by transient rearrangements of the electric field during deactivation. Such dynamic changes in the local field have been experimentally observed in the Shaker VSD (Asamoah et al., 2003).

The search for the molecular mechanisms of the two Trp mutants led us to modify the side chain at positions I241 and F244 using nonnaturals indole derivatives. Although our results could not confirm the involvement of cation-Π interactions at either site, they show a clear participation of the indole nitrogen of I241W, but not F244W, in the large positive shift of the voltage required to open the channel's pore. These results, however, did not help us to draw simple hypotheses for the mutant phenotypes. Therefore, to shed light on these mechanisms we aimed at studying in silico how these Trp side chains could stabilize an intermediate VSD conformation. To this end, we first determined a computational pathway of the WT Kv1.2 VSD transition by using the string method connecting two structural models of the up and down states.

Models of the up and down state of the VSD

A prerequisite for using the string method to determine a transition pathway is to have atomic models for each of the two end-point states that are reasonably accurate. In the present study, the up and down states of the VSD were taken from long MD simulations with explicit solvent and membrane (Khalili-Araghi et al., 2010). The initial VSD structure used to start these simulations were taken from the complete models that were previously generated by Pathak et al. (2007) using the Rosetta-Membrane structure prediction method. The up state structure essentially corresponds to the original x-ray coordinates of the Kv1.2 channel of Long et al.

(2005), upon which the missing atoms were added. Subsequent comparison with the x-ray structure of the Kv1.2/Kv2.1 chimera channel (Long et al., 2007) confirmed that the missing atoms of the up state were correctly modeled by the Rosetta-Membrane method. The down state structure is a model generated to satisfy the experimental observations known at the time. Subsequently, it was noted that the model was consistent with several additional experimental constraints that had not been used in the original modeling (Campos et al., 2007; Vargas et al., 2011). A recent comparison of all available atomic models of the down (resting) state of the VSD shows that they all lie within ∼3.5 Å RMS (backbone Cα) relative to one another revealing the emergence of a strong consensus on this issue among the different groups (Vargas et al., 2012). Specifically, the down state considered here corresponds to the "closed state C3" of Henrion et al. (2012), the "penultimate resting state" of Delemotte et al. (2011).

Thus, the model used here is likely to represent the "default" down state of the VSD that is most populated under normal physiological conditions with a moderate negative membrane potential (Delemotte et al., 2011; Henrion et al., 2012). A deeper resting state (referred to as C4) appear to also exist, with S4 further translated toward the intracellular side, which can be reached after long hyperpolarization (Delemotte et al., 2011; Henrion et al., 2012). This is the final conformation reached after spontaneous transition observed in extremely long MD simulations with a large negative membrane potential (Jensen et al., 2012). Therefore, although the structure of the resting state of the VSD has not been determined to atomic resolution and there remains some disparity between the proposed models, we believe that the overall conformation of the resting state of the VSD is not controversial anymore. The information currently available, together with advanced computational modeling techniques, is sufficient to broadly outline the VSD resting state conformation within ∼3–4 Å RMS (Vargas et al., 2012). Such accuracy is sufficient for a meaningful application of the string method. Moreover, the remaining uncertainty about the accuracy of the resting state and the possible importance of a deeper resting state of the VSD do not bear on the present analysis. Ultimately, the relevance of the present pathway lies in its ability to explain the occurrence of the experimentally detected intermediate VSD conformation stabilized by the I241W mutation. Repeating the string calculation by starting from a deeper resting state C4 would not affect our conclusions as long as this intermediate conformation occurs along the pathway between the two end-points considered here.
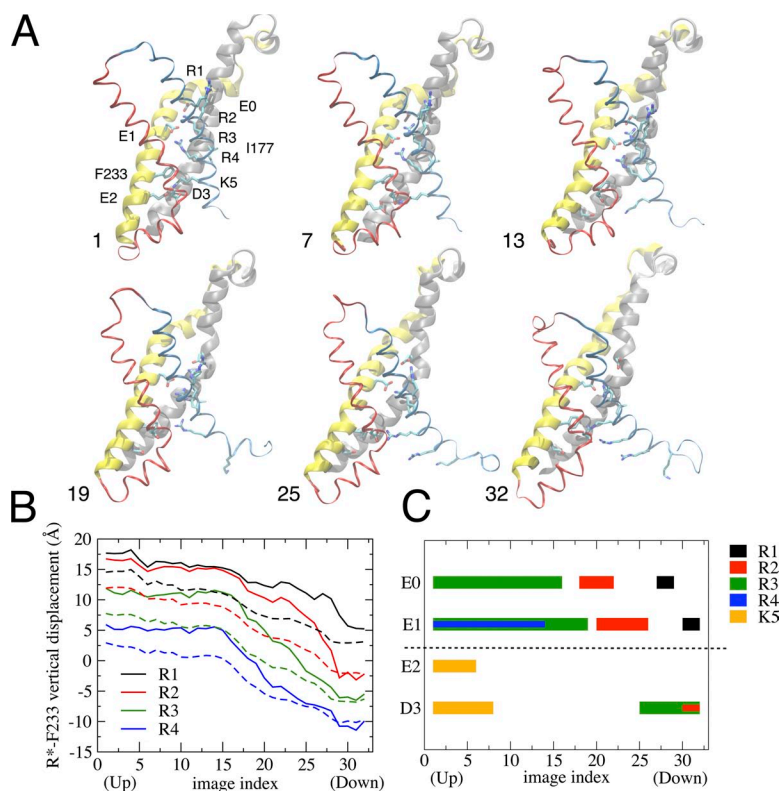
Simulation of the VSD transition

A molecular model of the transition pathway using the aforementioned models of the down and up states

(Khalili-Araghi et al., 2010) was built using a computational approach called the string method with swarms-of-trajectories. The string method is a well-established algorithm designed to compute optimal reaction pathways in systems comprising a large number of degrees of freedom (E et al., 2005; Maragliano et al., 2006), and it has been applied extensively to compute large scale conformational transitions in proteins (Miller et al., 2007; Zhu and Hummer, 2010; Ovchinnikov et al., 2011; Kirmizialtin et al., 2012). The version using swarms-of-trajectories was introduced by Pan et al. (2008) and first applied to study Src kinase activation (Gan et al., 2009). Fig. S2 A shows the averaged path-RMSD during string relaxation and Fig. S2 B shows the RMSD of the images along the path at consecutive iterations. It can be observed that the images at the center of the path are those that evolved and relax the most during the iterations. A similar behavior was observed in other string method applications and this is, indeed, expected when the initial path is generated by targeted MD simulations, because the central images are likely to start from the least favorable configurations in such conditions. Atomic details in the conformational transition were obtained from the converged path. The 32 images forming the string provide a sequence of representative atomic-detailed conformational snapshots along the transition pathway. Fig. 9 A depicts few representative snapshots of the VSD conformations along the converged path. A protein database file containing all 32 images for the VSD conformational transition is provided in supplementary information.

The mechanism that emerges from the analysis of the conformational change is consistent with the helical-screw/sliding-helix model: the S4 helix is the VSD region that experiences the largest conformational change. During the de-activation transition (up to down state), S4 moves along its main axis toward the intracellular side without essential alteration of the secondary structure, and rotates around its axis while the gating residues translate across the membrane. The transition can be characterized by the sequential passing of the S4 residues across the position of F233 (F290 in Shaker) on S2. The z position of the S4 arginines Cα and Cζ atoms with respect to F233 along the optimized path is shown in Fig. 9 B. The first residue to pass is R4, followed by R3 and R2. Relative to F233, residues R2, R3, and R4 move ~17 Å measured by their Cζ positions and ~14 Å measured by their Cα positions. The S4 movement halts before R1 passes the level of F233. Another relevant feature along the path is the sequential formation of salt bridges between the gating S4 residues and their counterparts on the facing helices, shown in Fig. 9 C. The voltage-gating motion, obtained here by the string method, is broadly consistent with the previous results from Henrion et al. (2012) and Delemotte et al. (2011), as well as with the spontaneous transition observed in extremely long MD simulations driven by a large negative membrane potential (Jensen et al., 2012).

Figure 9. Simulation of the VSD trajectory using the string method. (A) The figure shows selected snapshots of VSD conformations along the converged path from the string method. The numbers indicate the positions from the initial linear path between the up (image #1) and down (image #32) states. The coloring method for S1–S4 is the same as in Fig. 1 A. The side chains of F233 (F290 in Shaker), I177 (I241 in Shaker) E0-2, D3, and R1–R4 are shown in all snapshots in licorice representation. (B) Vertical Z-distance of the S4 arginines relative to the center-of-mass of F233 side chain along the optimized path. The solid and dashed lines correspond to the distance relative to the R1–4 Cζ and R1–4 Cα, respectively. (C) Transient salt bridges analysis along the optimized path; according to the color code, a color corresponding to a particular arginine/lysine is drawn at an image if in the corresponding configuration there is a salt bridge between the basic and the acidic residue. The index of the images along the path is reported on the x-axis, and the acidic amino acids making interactions with the S4 arginines are reported on the y-axis. The horizontal dashed line schematically separates the extracellular region (above) from the intracellular (below).
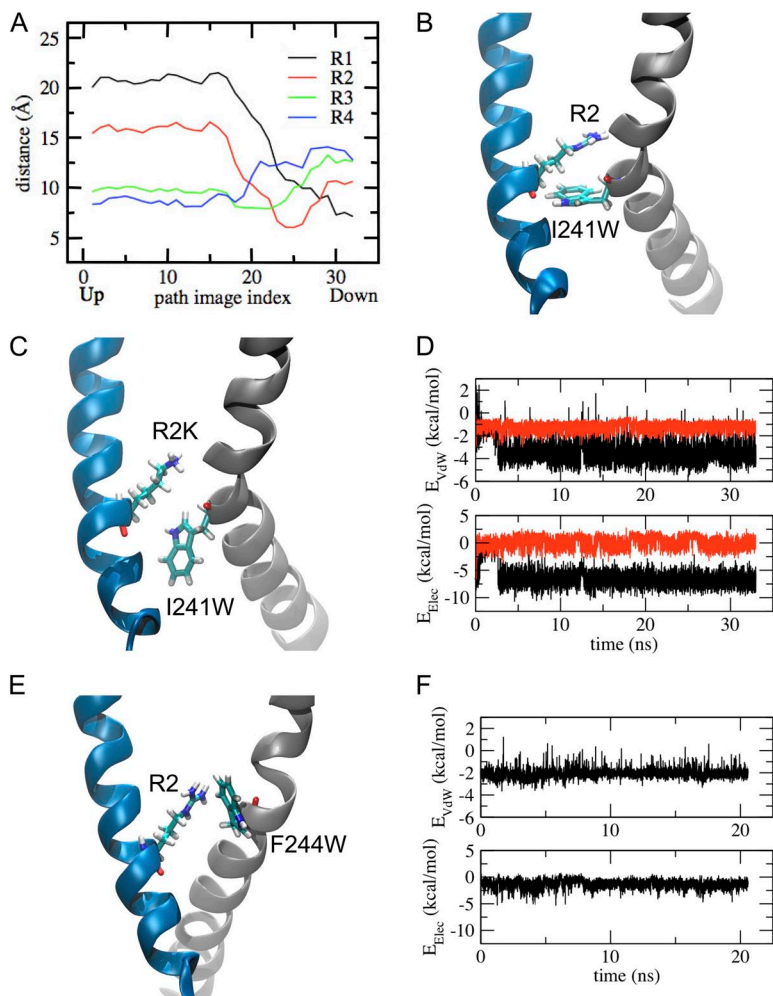
A possible molecular mechanism for the I241W and F244W phenotypes

Along the calculated transition pathway, it is observed that the Cβ of I241 (I177 in Kv1.2) moves closer to the R2 Cζ than any of the other gating charges (Fig. 10 A), in good agreement with the hypothesis of an interaction between I241W and R2 in an intermediate state. This observation is not at odds with the previously reported atomic proximity between 241 and R1 as (1) this proximity was assessed by disulfide locking experiments in which the native Arg and Ile were replaced by relatively shorter Cys side chains and (2) occurred in the resting state (Campos et al., 2007).

In an attempt to identify possible interactions underlying the functional phenotype of the I241W mutation, the intermediate configuration with the minimal Cβ-Cζ distance between I241 and R2 (image #25) was extracted from the computational pathway, the Ile at position 241 was mutated into a Trp, and the resulting system was simulated for 32 ns. It should be clear that, for the purpose of characterizing the interactions of one specific intermediate state, there is no need to generate simulation of durations equivalent to the time-course of
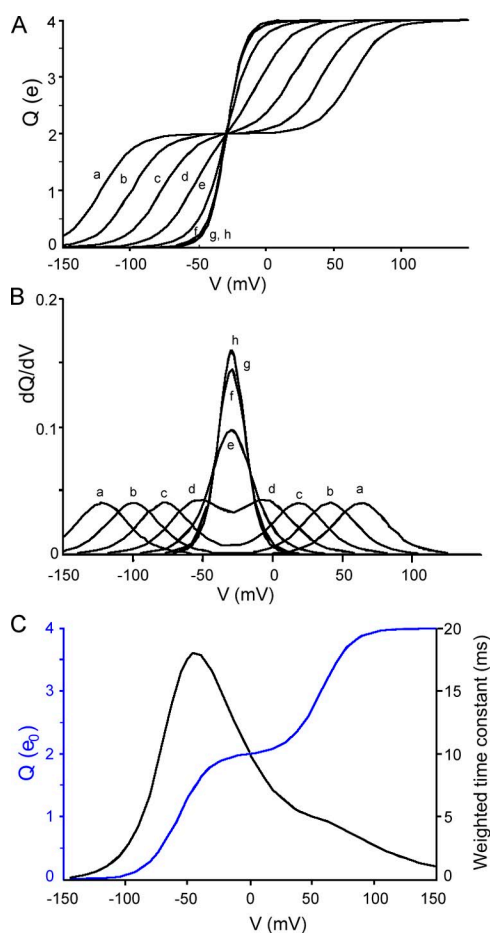
the complete VSD conformational transition (i.e., milliseconds). Rather, as the conformation of the VSD backbone in this intermediate state is parametrically restrained via the values of the collective variables z during the simulation, the computational time only needs to be sufficiently long to allow slight side chains rotameric rearrangements, which typically occur within pico- to nano-second time scale. Moreover, this simulation aims at studying how I241W stabilizes the intermediate state, not how I241W may alter late gating transitions near the open state. Thus the presence of the central pore domain is not necessary for this MD simulation of the intermediate state within the VSD.

The simulation shows that the Trp side chain of the mutant I241W adopts an orientation such that the N-H group of the indole ring is within hydrogen bonding distance toward the backbone carbonyl oxygen of R2 (Fig. 10 B). It is somewhat surprising regarding these observations that the robust Q-V split mediated by I241W seems to be maintained in presence of the R2Q mutation (Fig. S1), but not in presence of the R2K mutation (Fig. 5 B). We thus inserted the double mutation I241W/R2K in the same intermediate state described

Figure 10. A possible mechanism for the I241W and F244W phenotypes. (A) Graph showing the distances between I241 (Cβ) and R1–R4 (Cζ) along the pathway obtained by the string method. The mutations I241W (B) and I241W/R2K (C) were independently introduced in silico in the conformation having the minimal I241-R2 distance (image #25) and equilibrated for 32 ns. Only the side chains were allowed to move during the two equilibrations. (D) The graph shows the vdW (top) and electrostatic (bottom) interaction energies between I241W and R2 (black) or between I241W and R2K (red) during the two simulations. (E) The mutation F244W was introduced in silico in image #22 giving the minimal F244-R2 (Cβ-Cζ) distance and equilibrated for 20 ns. The cartoon shows the side chains of R2 and F244W after equilibration. (F) The graph shows the vdW (top) and electrostatic (bottom) interaction energies between F244W and R2 during the simulation.

above and equilibrated the side chains for 32 ns. The simulation shows that the rotamer of the Trp observed in the single mutant I241W becomes unstable and rapidly flips in the presence of the second mutation R2K, pointing the nitrogen away from the backbone carbonyl of S4 (Fig. 10 C). These simulations show a strong interaction energy of about -10 kcal/mol for the interacting pair I241W/R2, with average vdW and electrostatic components of -3.5 kcal/mol and -6.8 kcal/mol, respectively (Fig. 10 D, black traces). However, the average interaction energy for the pair I241W/R2K is only about -1.2 kcal/mol, mostly from vdW interactions (Fig. 10 D, red trace). Hence, the computational analysis predicts, in agreement with our functional data, the
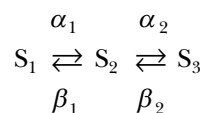
formation of a hydrogen bond between the N-H indole moiety of I241W along S1 and the backbone carbonyl oxygen of R2, stabilizing an intermediate state along the calculated VSD pathway. The R2K mutation seems to favor a different rotamer for I241W that abrogates the formation of the hydrogen bond, thus providing a possible molecular mechanism for the absence of a strong intermediate state stabilization in the I241W/ R2K mutant. Because the I241W phenotype persists in the double mutant I241W/R2Q, it is possible that, in contrast to R2K, R2Q does not prevent the nitrogen atom of I241W to engage into a hydrogen bond with the backbone carbonyl of R2Q.

To investigate the mechanism of F244W, we extracted the image showing the minimal Cβ-Cζ distance between F244 (F180 in Kv1.2) and R2 from the calculated overall path (image #22). As expected from the phenotypic similarity between I241W and F244W channels, this computed intermediate conformation is very close to the one giving the shortest I241-R2 Cβ-Cζ distance, with a RMSD difference of only 1.35 Å. We next created the F244W mutant in silico and simulated the structure for 20 ns. The results show that the Trp rotamer is located within atomic proximity to the guanidinium group of R2 (Fig. 10 E), with a moderate Arg–Trp interaction energy (-3.3 kcal/mol) resulting mostly from the nonpolar van der Waals interactions (-2.1 kcal/mol on average; Fig. 10 F). Because the amino group of the Lys side chain is smaller than the guanidinium group of Arg, a possible explanation of the diminished Q-V split in the F244W/R2K mutant may be a decrease interaction surface between the Trp and Lys side chains.

In summary, we report evidence for an intermediate state of the VSD occurring during activation and deactivation gating. The existence of this intermediate state is consistent with the computational transition pathway predicted by the string method between models of the up and down state of the voltage sensor. Our combination of experimental results and MD simulations suggest a possible structural mechanism for the stabilization of this intermediate state in which the indole nitrogen of I241W may form a hydrogen bond with the backbone carbonyl oxygen of R2. The present effort demonstrates the strength of a multidisciplinary approach to understand the complexity and dynamics of the conformational changes in voltage sensor domains.

APPENDIX

A simple 3-state model of charge movement may be used as a minimal model to analyze and interpret the results presented in this paper:

$$S_1 \underset{\beta_1}{\overset{\alpha_1}{\rightleftarrows}} S_2 \underset{\beta_2}{\overset{\alpha_2}{\rightleftarrows}} S_3$$

Figure 11. Simulations with the 3-state model. (A) Q-V curves computed for several values of K_1 and K_2, as follows (a): $K_1 = 0.0001$, $K_2 = 166.7$, $s = 14.8$; (b): $K_1 = 0.0004$, $K_2 = 27.8$, $s = 11.2$; (c): $K_1 = 0.0022$, $K_2 = 4.63$, $s = 7.67$; (d): $K_1 = 0.013$, $K_2 = 0.77$, $s = 4.09$; (e): $K_1 = 0.078$, $K_2 = 0.129$, $s = 0.5$. The next three curves are (f): $K_1 = 0.467$, $K_2 = 0.021$, $s = -3.08$; (g): $K_1 = 2.8$, $K_2 = 0.0036$, $s = -6.66$; and (h): $K_1 = 16.8$, $K_2 = 0.0006$, $s = -10.25$. Curves e–h can be well fit by a single Boltzmann given apparent valences of 2.36, 3.54, 3.91, and 3.99, respectively. (B) First derivative of the Q-V curves shown in part A. (C) Q-V and weighted time constant versus V curves computed with the 3-state model with the following parameters: $z_{1f} = 0.5$, $z_{1b} = 1.5$, $z_{2f} = 1.2$, $z_{2b} = 0.8$, $\alpha_{10} = 0.1$, $\beta_{10} = 0.001$, $\alpha_{20} = 0.001$, $\beta_{20} = 0.1$.

With the rates given by:

$$\alpha_i = \alpha_{i0}\exp\left(\frac{z_{if}\,e_0 V}{kT}\right)$$

$$\beta_i = \beta_{i0}\exp\left(\frac{-z_{ib}\,e_0 V}{kT}\right), \quad i = 1, 2,$$

where α_{i0} and β_{i0} are the rates at voltage $V = 0$ mV and z_{if} and z_{ib} are the forward and backward valences, respectively, both positive. The charge transferred between S_1 and S_2 is $e_0(z_{1f} + z_{1b})$ and between S_2 and S_3 is $e_0(z_{2f} + z_{2b})$; k, T, and e_0 are the Boltzmann constant, absolute temperature, and electronic charge, respectively. Defining $K_1 = \beta_1/\alpha_1$ and $K_2 = \beta_2/\alpha_2$, and $z_1 = z_{1f} + z_{1b}$ and $z_2 = z_{2f} + z_{2b}$, the Q-V is given by

$$Q(V) = N\frac{z_2 + z_1(\mathrm{E}_2 + 1)}{1 + \mathrm{E}_2(1 + \mathrm{E}_1)},$$

where N is the number of sensors and E_1, E_2, V_1, and V_2 are given by

$$\mathrm{E}_1 = \exp\left(-\frac{z_1 e_o(V - V_1)}{kT}\right), \mathrm{E}_2 = \exp\left(-\frac{z_2 e_0(V - V_2)}{kT}\right),$$

$$V_1 = \frac{kT}{z_1 e_0}\ln K_1 \ \text{ and } \ V_2 = \frac{kT}{z_2 e_0}\ln K_2.$$

The condition to stabilize S_2, which produces a split in the Q-V, is that

$$K_1 \ll 1 \text{ and } K_2 \gg 1,$$

which translates into a criterion s given by

$$s = (V_2 z_2 - V_1 z_1)\frac{e_0}{kT} \gg 0.$$

A family of curves with different values of s is plotted in Fig. 11 A. As s becomes more positive the more pronounced becomes the split of the Q-V, as judged by the first derivative with respect to V of the Q-V curve, as shown in Fig. 11 B. As the value of s becomes less positive (Fig. 11, curves a through e) the split tends to disappear and the Q-V curves may be fitted by a 2-state model (also called a simple Boltzmann), but the fitted valence is always less than the total valence. In the limit when the value of s is very negative the fitted apparent valence approaches the total valence (4 in this example).

The general solution of the 3-state model contains three eigenvalues, where one of them is always 1. Thus, the gating currents have in general two time constants

but the coefficients of the exponentials depend on the relative rates and valences between states. The experimentally recorded gating currents show at least two exponential decays that have been characterized in this paper as a single weighted average. A solution of the 3-state model with conditions that produce a split in the Q-V curve is shown in Fig. 11 C, along with the computed weighted average time constant of the gating current decay as a function of membrane potential. The two bell-shaped time constants as a function of voltage of the model are reproduced in this particular simulation as a main peak and a shoulder in agreement with the experimental observation.

To reproduce all the kinetic features of the gating current at least one more state must be added because some of the recorded gating currents show a rising phase, indicating that there is at least one more eigenvalue.

REFERENCES

Aggarwal, S.K., and R. MacKinnon. 1996. Contribution of the S4 segment to gating charge in the Shaker K+ channel. *Neuron.* 16:1169–1177. http://dx.doi.org/10.1016/S0896-6273(00)80143-9

Ahern, C.A., and R. Horn. 2005. Focused electric field across the voltage sensor of potassium channels. *Neuron.* 48:25–29. http://dx.doi.org/10.1016/j.neuron.2005.08.020

Ahern, C.A., A.L. Eastwood, H.A. Lester, D.A. Dougherty, and R. Horn. 2006. A cation-pi interaction between extracellular TEA and an aromatic residue in potassium channels. *J. Gen. Physiol.* 128:649–657. http://dx.doi.org/10.1085/jgp.200609654

Ahern, C.A., A.L. Eastwood, D.A. Dougherty, and R. Horn. 2008. Electrostatic contributions of aromatic residues in the local anesthetic receptor of voltage-gated sodium channels. *Circ. Res.* 102:86–94. http://dx.doi.org/10.1161/CIRCRESAHA.107.160663

Armstrong, C.M., and F. Bezanilla. 1973. Currents related to movement of the gating particles of the sodium channels. *Nature.* 242:459–461. http://dx.doi.org/10.1038/242459a0

Asamoah, O.K., J.P. Wuskell, L.M. Loew, and F. Bezanilla. 2003. A fluorometric approach to local electric field measurements in a voltage-gated ion channel. *Neuron.* 37:85–97. http://dx.doi.org/10.1016/S0896-6273(02)01126-1

Belokon, Y.N., S. Harutyunyan, E.V. Vorontsov, A.S. Peregudov, V.N. Chrustalev, K.A. Kochetkov, D. Pripadchev, A.S. Sagyan, A.K. Beck, and D. Seebach. 2004. Nucleophilic addition to an achiral dehydroalanine Schiff base Ni(II) complex as a route to amino

acids. A case of stereodetermining asymmetric protonation in the presence of TADDOL. *Arkivoc*. 3:132–150.

Ben-Chaim, Y., B. Chanda, N. Dascal, F. Bezanilla, I. Parnas, and H. Parnas. 2006. Movement of 'gating charge' is coupled to ligand binding in a G-protein-coupled receptor. *Nature*. 444:106–109. http://dx.doi.org/10.1038/nature05259

Bezanilla, F., and E. Stefani. 1996. Gating of the shaker B potassium channel. *In* Basic Neuroscience in Invertebrates. Vol. 1. H. Koike, editor Japan Scientific Societies Press, Tokyo.

Campos, F.V., B. Chanda, B. Roux, and F. Bezanilla. 2007. Two atomic constraints unambiguously position the S4 segment relative to S1 and S2 segments in the closed state of Shaker K channel. *Proc. Natl. Acad. Sci. USA*. 104:7904–7909. http://dx.doi.org/10.1073/pnas.0702638104

Cha, A., and F. Bezanilla. 1997. Characterizing voltage-dependent conformational changes in the Shaker K+ channel with fluorescence. *Neuron*. 19:1127–1140. http://dx.doi.org/10.1016/S0896-6273(00)80403-1

Chen, X., Q. Wang, F. Ni, and J. Ma. 2010. Structure of the full-length Shaker potassium channel Kv1.2 by normal-mode-based X-ray crystallographic refinement. *Proc. Natl. Acad. Sci. USA*. 107:11352–11357. http://dx.doi.org/10.1073/pnas.1000142107

Darden, T., D. York, and L. Pedersen. 1993. Particle mesh Ewald. An Nlog(N) method for Ewald sums in large systems. *J. Chem. Phys.* 98:10089–10092. http://dx.doi.org/10.1063/1.464397

DeCaen, P.G., V. Yarov-Yarovoy, Y. Zhao, T. Scheuer, and W.A. Catterall. 2008. Disulfide locking a sodium channel voltage sensor reveals ion pair formation during activation. *Proc. Natl. Acad. Sci. USA*. 105:15142–15147. http://dx.doi.org/10.1073/pnas.0806486105

DeCaen, P.G., V. Yarov-Yarovoy, E.M. Sharp, T. Scheuer, and W.A. Catterall. 2009. Sequential formation of ion pairs during activation of a sodium channel voltage sensor. *Proc. Natl. Acad. Sci. USA*. 106:22498–22503. http://dx.doi.org/10.1073/pnas.0912307106

DeCaen, P.G., V. Yarov-Yarovoy, T. Scheuer, and W.A. Catterall. 2011. Gating charge interactions with the S1 segment during activation of a Na+ channel voltage sensor. *Proc. Natl. Acad. Sci. USA*. 108:18825–18830. http://dx.doi.org/10.1073/pnas.1116449108

Delemotte, L., M. Tarek, M.L. Klein, C. Amaral, and W. Treptow. 2011. Intermediate states of the Kv1.2 voltage sensor from atomistic molecular dynamics simulations. *Proc. Natl. Acad. Sci. USA*. 108:6109–6114. http://dx.doi.org/10.1073/pnas.1102724108

Dougherty, D.A. 1996. Cation-pi interactions in chemistry and biology: a new view of benzene, Phe, Tyr, and Trp. *Science*. 271:163–168. http://dx.doi.org/10.1126/science.271.5246.163

E, W., W. Ren, and E. Vanden-Eijnden. 2005. String method for the study of rare events. *J. Phys. Chem. B*. 109:6688–6693.

Feller, S.E. 2000. Molecular dynamics simulations of lipid bilayers. *Curr. Opin. Colloid Interface Sci.* 5:217–223. http://dx.doi.org/10.1016/S1359-0294(00)00058-3

Gan, W., S. Yang, and B. Roux. 2009. Atomistic view of the conformational activation of Src kinase using the string method with swarms-of-trajectories. *Biophys. J.* 97:L8–L10. http://dx.doi.org/10.1016/j.bpj.2009.06.016

Haddad, G.A., and R. Blunck. 2011. Mode shift of the voltage sensors in Shaker K+ channels is caused by energetic coupling to the pore domain. *J. Gen. Physiol.* 137:455–472. http://dx.doi.org/10.1085/jgp.201010573

Henrion, U., J. Renhorn, S.I. Börjesson, E.M. Nelson, C.S. Schwaiger, P. Bjelkmar, B. Wallner, E. Lindahl, and F. Elinder. 2012. Tracking a complete voltage-sensor cycle with metal-ion bridges. *Proc. Natl. Acad. Sci. USA*. 109:8552–8557. http://dx.doi.org/10.1073/pnas.1116938109

Hodgkin, A.L., and A.F. Huxley. 1952. A quantitative description of membrane current and its application to conduction and excitation in nerve. *J. Physiol.* 117:500–544.

Islas, L.D., and F.J. Sigworth. 2001. Electrostatics and the gating pore of Shaker potassium channels. *J. Gen. Physiol.* 117:69–89. http://dx.doi.org/10.1085/jgp.117.1.69

Jacobson, D.A., F. Mendez, M. Thompson, J. Torres, O. Cochet, and L.H. Philipson. 2010. Calcium-activated and voltage-gated potassium channels of the pancreatic islet impart distinct and complementary roles during secretagogue induced electrical responses. *J. Physiol.* 588:3525–3537. http://dx.doi.org/10.1113/jphysiol.2010.190207

Jensen, M.O., V. Jogini, D.W. Borhani, A.E. Leffler, R.O. Dror, and D.E. Shaw. 2012. Mechanism of voltage gating in potassium channels. *Science*. 336:229–233. http://dx.doi.org/10.1126/science.1216533

Jorgensen, W.L., J. Chandrasekhar, J.D. Madura, R.W. Impey, and M.L. Klein. 1983. Comparison of simple potential functions for simulating liquid water. *J. Chem. Phys.* 79:926–935. http://dx.doi.org/10.1063/1.445869

Khalili-Araghi, F., V. Jogini, V. Yarov-Yarovoy, E. Tajkhorshid, B. Roux, and K. Schulten. 2010. Calculation of the gating charge for the Kv1.2 voltage-activated potassium channel. *Biophys. J.* 98:2189–2198. http://dx.doi.org/10.1016/j.bpj.2010.02.056

Kirmizialtin, S., V. Nguyen, K.A. Johnson, and R. Elber. 2012. How conformational dynamics of DNA polymerase select correct substrates: experiments and simulations. *Structure*. 20:618–627. http://dx.doi.org/10.1016/j.str.2012.02.018

Lacroix, J.J., and F. Bezanilla. 2011. Control of a final gating charge transition by a hydrophobic residue in the S2 segment of a K+ channel voltage sensor. *Proc. Natl. Acad. Sci. USA*. 108:6444–6449. http://dx.doi.org/10.1073/pnas.1103397108

Lacroix, J.J., A.J. Labro, and F. Bezanilla. 2011. Properties of deactivation gating currents in Shaker channels. *Biophys. J.* 100:L28–L30. http://dx.doi.org/10.1016/j.bpj.2011.01.043

Lin, M.C., J. Abramson, and D.M. Papazian. 2010. Transfer of ion binding site from ether-a-go-go to Shaker: Mg2+ binds to resting state to modulate channel opening. *J. Gen. Physiol.* 135:415–431. http://dx.doi.org/10.1085/jgp.200910320

Lin, M.C., J.Y. Hsieh, A.F. Mock, and D.M. Papazian. 2011. R1 in the Shaker S4 occupies the gating charge transfer center in the resting state. *J. Gen. Physiol.* 138:155–163. http://dx.doi.org/10.1085/jgp.201110642

Long, S.B., E.B. Campbell, and R. MacKinnon. 2005. Crystal structure of a mammalian voltage-dependent Shaker family K+ channel. *Science*. 309:897–903.

Long, S.B., X. Tao, E.B. Campbell, and R. MacKinnon. 2007. Atomic structure of a voltage-dependent K+ channel in a lipid membrane-like environment. *Nature*. 450:376–382. http://dx.doi.org/10.1038/nature06265

Mackerell, A.D. Jr., M. Feig, and C.L. Brooks III. 2004. Extending the treatment of backbone energetics in protein force fields: limitations of gas-phase quantum mechanics in reproducing protein conformational distributions in molecular dynamics simulations. *J. Comput. Chem.* 25:1400–1415. http://dx.doi.org/10.1002/jcc.20065

Mannuzzu, L.M., M.M. Moronne, and E.Y. Isacoff. 1996. Direct physical measure of conformational rearrangement underlying potassium channel gating. *Science*. 271:213–216. http://dx.doi.org/10.1126/science.271.5246.213

Maragliano, L., A. Fischer, E. Vanden-Eijnden, and G. Ciccotti. 2006. String method in collective variables: minimum free energy paths and isocommittor surfaces. *J. Chem. Phys.* 125:24106. http://dx.doi.org/10.1063/1.2212942

Martyna, G.J., D.J. Tobias, and M.L. Klein. 1994. Constant pressure molecular dynamics algorithms. *J. Chem. Phys.* 101:4177–4189. http://dx.doi.org/10.1063/1.467468

Miller, T.F. III, E. Vanden-Eijnden, and D. Chandler. 2007. Solvent coarse-graining and the string method applied to the hydrophobic

collapse of a hydrated chain. *Proc. Natl. Acad. Sci. USA.* 104:14559–14564. http://dx.doi.org/10.1073/pnas.0705830104

Murata, Y., H. Iwasaki, M. Sasaki, K. Inaba, and Y. Okamura. 2005. Phosphoinositide phosphatase activity coupled to an intrinsic voltage sensor. *Nature.* 435:1239–1243. http://dx.doi.org/10.1038/nature03650

Muroi, Y., M. Arcisio-Miranda, S. Chowdhury, and B. Chanda. 2010. Molecular determinants of coupling between the domain III voltage sensor and pore of a sodium channel. *Nat. Struct. Mol. Biol.* 17:230–237. http://dx.doi.org/10.1038/nsmb.1749

Ovchinnikov, V., M. Karplus, and E. Vanden-Eijnden. 2011. Free energy of conformational transition paths in biomolecules: the string method and its application to myosin VI. *J. Chem. Phys.* 134:085103. http://dx.doi.org/10.1063/1.3544209

Pan, A.C., D. Sezer, and B. Roux. 2008. Finding transition pathways using the string method with swarms of trajectories. *J. Phys. Chem. B.* 112:3432–3440. http://dx.doi.org/10.1021/jp0777059

Pathak, M.M., V. Yarov-Yarovoy, G. Agarwal, B. Roux, P. Barth, S. Kohout, F. Tombola, and E.Y. Isacoff. 2007. Closing in on the resting state of the Shaker K(+) channel. *Neuron.* 56:124–140. http://dx.doi.org/10.1016/j.neuron.2007.09.023

Payandeh, J., T. Scheuer, N. Zheng, and W.A. Catterall. 2011. The crystal structure of a voltage-gated sodium channel. *Nature.* 475:353–358. http://dx.doi.org/10.1038/nature10238

Perozo, E., R. MacKinnon, F. Bezanilla, and E. Stefani. 1993. Gating currents from a nonconducting mutant reveal open-closed conformations in Shaker K+ channels. *Neuron.* 11:353–358. http://dx.doi.org/10.1016/0896-6273(93)90190-3

Petheo, G.L., A. Orient, M. Baráth, I. Kovács, B. Réthi, A. Lányi, A. Rajki, E. Rajnavölgyi, and M. Geiszt. 2010. Molecular and functional characterization of Hv1 proton channel in human granulocytes. *PLoS ONE.* 5:e14081. http://dx.doi.org/10.1371/journal.pone.0014081

Phillips, J.C., R. Braun, W. Wang, J. Gumbart, E. Tajkhorshid, E. Villa, C. Chipot, R.D. Skeel, L. Kalé, and K. Schulten. 2005. Scalable molecular dynamics with NAMD. *J. Comput. Chem.* 26:1781–1802. http://dx.doi.org/10.1002/jcc.20289

Pless, S.A., J.D. Galpin, A. Frankel, and C.A. Ahern. 2011a. Molecular basis for class Ib anti-arrhythmic inhibition of cardiac sodium channels. *Nat Commun.* 2:351. http://dx.doi.org/10.1038/ncomms1351

Pless, S.A., J.D. Galpin, A.P. Niciforovic, and C.A. Ahern. 2011b. Contributions of counter-charge in a potassium channel voltage-sensor domain. *Nat. Chem. Biol.* 7:617–623. http://dx.doi.org/10.1038/nchembio.622

Pless, S.A., A.P. Hanek, K.L. Price, J.W. Lynch, H.A. Lester, D.A. Dougherty, and S.C. Lummis. 2011c. A cation-π interaction at a phenylalanine residue in the glycine receptor binding site is conserved for different agonists. *Mol. Pharmacol.* 79:742–748. http://dx.doi.org/10.1124/mol.110.069583

Posson, D.J., and P.R. Selvin. 2008. Extent of voltage sensor movement during gating of shaker K+ channels. *Neuron.* 59:98–109. http://dx.doi.org/10.1016/j.neuron.2008.05.006

Posson, D.J., P. Ge, C. Miller, F. Bezanilla, and P.R. Selvin. 2005. Small vertical movement of a K+ channel voltage sensor measured with luminescence energy transfer. *Nature.* 436:848–851. http://dx.doi.org/10.1038/nature03819

Ramsey, I.S., M.M. Moran, J.A. Chong, and D.E. Clapham. 2006. A voltage-gated proton-selective channel lacking the pore domain. *Nature.* 440:1213–1216. http://dx.doi.org/10.1038/nature04700

Ruta, V., J. Chen, and R. MacKinnon. 2005. Calibrated measurement of gating-charge arginine displacement in the KvAP voltage-dependent K+ channel. *Cell.* 123:463–475. http://dx.doi.org/10.1016/j.cell.2005.08.041

Sasaki, M., M. Takagi, and Y. Okamura. 2006. A voltage sensor-domain protein is a voltage-gated proton channel. *Science.* 312:589–592. http://dx.doi.org/10.1126/science.1122352

Seoh, S.A., D. Sigg, D.M. Papazian, and F. Bezanilla. 1996. Voltage-sensing residues in the S2 and S4 segments of the Shaker K+ channel. *Neuron.* 16:1159–1167. http://dx.doi.org/10.1016/S0896-6273(00)80142-7

Smith-Maxwell, C.J., J.L. Ledwell, and R.W. Aldrich. 1998. Role of the S4 in cooperativity of voltage-dependent potassium channel activation. *J. Gen. Physiol.* 111:399–420. http://dx.doi.org/10.1085/jgp.111.3.399

Starace, D.M., and F. Bezanilla. 2001. Histidine scanning mutagenesis of basic residues of the S4 segment of the shaker k+ channel. *J. Gen. Physiol.* 117:469–490. http://dx.doi.org/10.1085/jgp.117.5.469

Starace, D.M., and F. Bezanilla. 2004. A proton pore in a potassium channel voltage sensor reveals a focused electric field. *Nature.* 427:548–553. http://dx.doi.org/10.1038/nature02270

Tao, X., A. Lee, W. Limapichat, D.A. Dougherty, and R. MacKinnon. 2010. A gating charge transfer center in voltage sensors. *Science.* 328:67–73. http://dx.doi.org/10.1126/science.1185954

Vargas, E., F. Bezanilla, and B. Roux. 2011. In search of a consensus model of the resting state of a voltage-sensing domain. *Neuron.* 72:713–720. http://dx.doi.org/10.1016/j.neuron.2011.09.024

Vargas, E., V. Yarov-Yarovoy, F. Khalili-Aragi, W.A. Catterall, M.L. Klein, M. Tarek, E. Lindahl, K. Schulten, E. Perozo, F. Bezanilla, and B. Roux. 2012. An emerging consensus on voltage-dependent gating from computational modeling and molecular dynamics simulations. *J. Gen. Phys.* 140:587–594. http://dx.doi.org/10.1085/jgp.201210873

Villalba-Galea, C.A., W. Sandtner, D.M. Starace, and F. Bezanilla. 2008. S4-based voltage sensors have three major conformations. *Proc. Natl. Acad. Sci. USA.* 105:17600–17607. http://dx.doi.org/10.1073/pnas.0807387105

Zhong, W., J.P. Gallivan, Y. Zhang, L. Li, H.A. Lester, and D.A. Dougherty. 1998. From ab initio quantum mechanics to molecular neurobiology: a cation-pi binding site in the nicotinic receptor. *Proc. Natl. Acad. Sci. USA.* 95:12088–12093. http://dx.doi.org/10.1073/pnas.95.21.12088

Zhu, F., and G. Hummer. 2010. Pore opening and closing of a pentameric ligand-gated ion channel. *Proc. Natl. Acad. Sci. USA.* 107:19814–19819. http://dx.doi.org/10.1073/pnas.1009313107